SSR Journal of Engineering and Technology (SSRJET)

Homepage: https://ssrpublisher.com/ssrjet/

Volume 3, Issue 4, 2026 ISSN: 3049-0383

Numerical Analysis of Energy Dissipation in Stepped Spillways with Channel Slope between 8.9º and 26.6º

Okechukwu Ozueigbo & J.C. Agunwamba

Department of Civil Engineering, University of Nigeria, Nsukka

Received: *21.03.2026* | ***Accepted:*** *11.04.2026* | ***Published:*** *18.04.2026*

***Corresponding author:** Okechukwu Ozueigbo

DOI: *10.5281/zenodo.19639777*

Abstract **Original Research Article**

Dam-integrated stepped spillways function as hydraulic energy dissipators, engineered to attenuate the destructive potential of high-velocity flows that would otherwise induce severe scour at the downstream riverbed. The staircase-like geometry of these structures promotes turbulence and momentum transfer, progressively reducing the hydraulic energy carried by floodwaters before they reach the channel below. Prior research has extensively documented the erosive consequences of residual kinetic energy acting on the riverbed, with findings particularly emphasizing structures built on steep gradients surpassing 26.6°. Yet, the intermediate slope range of 8.9° to 26.6° has received comparatively little scholarly attention with respect to energy dissipation performance, representing a notable knowledge gap that constrains the reliable engineering of stepped spillways within this gradient category. Furthermore, the prevailing model for quantifying energy dissipation across varying slope angles incorporates a friction factor, f, that is inherently difficult to evaluate objectively and is frequently subject to designer interpretation. This study aims to furnish design guidance for stepped spillways within the 8.9° to 26.6° slope range, while simultaneously introducing an approach that eliminates dependence on the friction factor, f. Air-water flow experiments using phase-detection intrusive probes were conducted at a large-scale facility on stepped spillways spanning this slope range, with emphasis on transitional and skimming flow regimes. The resulting models for energy loss estimation yielded Pearson correlation coefficients between 0.79 and 0.99, demonstrating strong agreement with measured data. All outcomes were internally consistent. The proposed models are straightforward in application and offer improved predictive performance relative to existing approaches.

Keywords: Stepped Spillway, Energy Dissipation, Nappe Flow, Skimming Flow.

1. INTRODUCTION

Stepped spillways are hydraulic structures positioned at the crests of dams to attenuate kinetic energy and mitigate downstream riverbed erosion. Among the various configurations devised for hydraulic flow management, the stepped spillway stands out for its primary function of progressively dissipating the energy of descending water (Thorwarth, 2008; Peyras et al., 1992).

As an advanced hydraulic conveyance structure, the stepped spillway spans across reservoirs,

dams, and other water-retaining facilities, enabling safe and regulated discharge under a wide range of flow conditions (Chanson, 1997a).

Depending on site-specific design requirements and environmental context, spillways may be constructed from stone or concrete. Stone is frequently favored in natural or rural settings, whereas concrete is more commonly adopted for its structural durability and longevity (Rajaratnam, 1990). The visual character of stepped spillways, which resembles cascading natural waterfalls, can enhance the aesthetic value of dam facilities for visitors. Beyond aesthetics, these structures also fulfill agricultural roles, including irrigation and wastewater conveyance, through the combined action of gravity and natural flow aeration (Ozueigbo & Agunwamba, 2025; Sorensen, 1985).

Ozueigbo and Agunwamba (2023) note that the step geometry is intentionally calibrated — sufficiently gradual to limit turbulence, yet steep enough to subdivide the descending water into manageable flow units. A defining characteristic of the spillway is its stepped profile, encompassing step dimensions, channel inclination, and the total number of steps. As water advances down the stepped chute, a developing boundary layer originating at the crest eventually intersects the free surface, at which point air entrainment commences (Fig. 1). This aeration process assists in limiting erosion and contributes to further energy reduction (Ohtsu et al., 2004; Ozueigbo & Agunwamba, 2022).

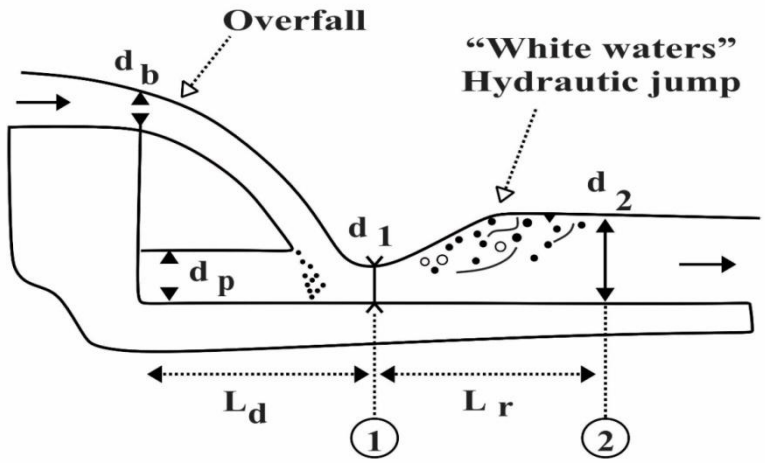

Figure 1. Nappe flow regime (Flow at a drop structure).

Unlike conventional smooth-surface spillways that convey water in a continuous sheet, stepped spillways direct flow across a succession of horizontal treads, which collectively impede the flow and substantially reduce its erosive capacity by replicating the behavior of natural stepped terrain or cascading waterfalls. The resulting velocity reduction and energy dissipation not only permit the use of smaller stilling basins at the spillway toe but also lower maintenance requirements, reduce repair frequency, and afford protection against erosive damage at both the structure base and the natural channel downstream (Chamani & Rajaratnam, 1994; Stefan & Chanson, 2014; Ozueigbo, 2022).

Stepped spillways represent a practical and technically advantageous solution for hydraulic flow management across a broad spectrum of infrastructure applications (Essery & Horner,

2005). Beyond their aesthetic contribution, they provide measurable benefits including reduced erosion potential, effective energy dissipation, and minimized long-term maintenance demands. Given the growing emphasis on sustainable water management in civil engineering practice, stepped spillways are anticipated to see wider adoption in future infrastructure projects (Thorwarth).

Considerable research effort has been directed at quantifying energy losses in flat stepped spillways operating at channel slopes of 26.6° or steeper (Ozueigbo, 2025). By contrast, energy dissipation in stepped spillways with inclinations between 26.6° and 3.4° has attracted far fewer investigations.

Consequently, a significant gap persists in the knowledge base underpinning the design methodology for this slope category (Ozueigbo, 2025).

Additionally, the prevailing energy loss model for stepped spillways incorporates the friction factor, f, as a key parameter. This variable is inherently difficult to determine with precision and is often assigned based on subjective designer judgment. Accordingly, the primary objectives of this study are twofold: to develop an energy dissipation model that eliminates the need for the friction factor, f, and to systematically examine energy dissipation in flat stepped spillways with channel slopes ranging from 8.9° to 26.6°.

Stephenson (1991) and Chanson (1997b) identified three distinct flow regimes over stepped spillways: nappe, transition, and skimming. Each regime exhibits unique hydraulic characteristics governed by discharge rate and step geometry. The nappe flow regime, as described by Chanson (1994), occurs at low discharges and is characterized by a freely falling water sheet that plunges from one step to the next, producing a sequence of small waterfalls (Fig. 2). The transitional flow regime, discussed by Degouite et al. (1992), is associated with moderate flow rates and is marked by pronounced surface spray and turbulence.

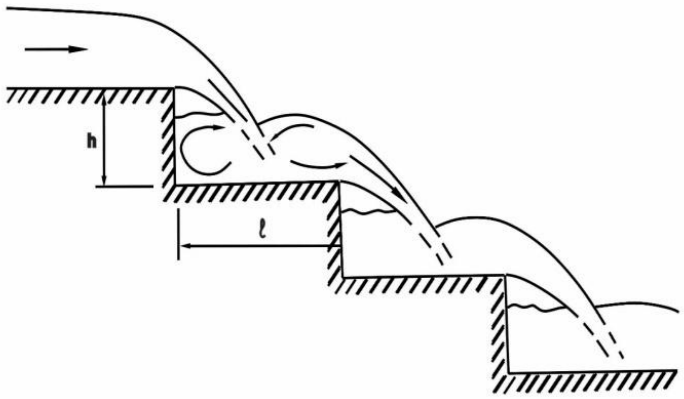

Figure 2: Nappe flow with partially developed hydraulic jump

At higher flow rates, the skimming flow regime develops, in which a coherent stream glides over the step edges while recirculating vortices occupy the cavities between steps and the primary flow (Chanson & Toombes, 2002a) (Figs. 3 and 4).

Each of the three flow regimes operates through a distinct energy dissipation mechanism, which may be quantified as follows, according to Chanson and Toombes (2002b):

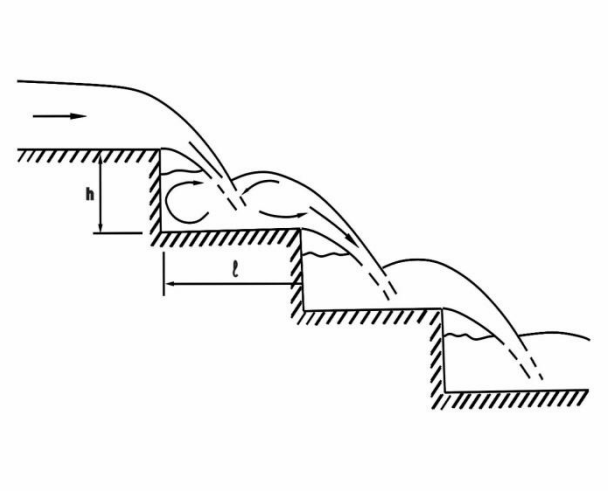

Figure 3. Skimming flow regime

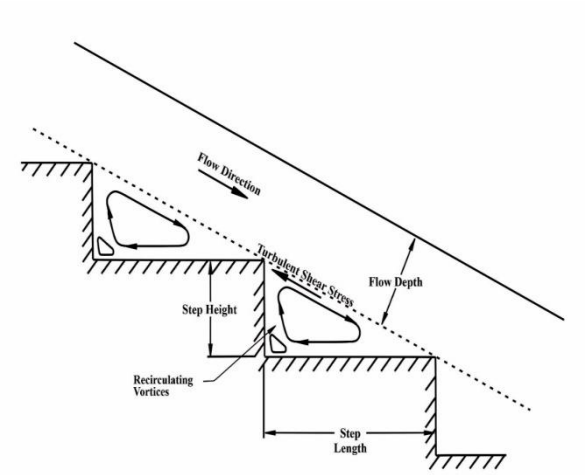

Figure 4. Skimming flow regime with uniform flow conditions

Energy Loss in Nappe Flow Regime

At any intermediate location along the spillway, the head loss equates to the energy dissipated within a nappe flow regime characterized by a fully developed hydraulic jump (Fig. 1). The aggregate head loss, ΔH, along the spillway equals the difference between the maximum upstream head, H_{xma}, and the residual head, H_{res}, at the spillway toe (Chanson, 1994, 1994a).

$$\frac{\Delta H}{H_{max}} = 1 - \frac{\frac{d_1}{d_c} + \frac{1}{2}\left(\frac{d_c}{d_1}\right)^2}{\frac{3}{2} + \frac{H_{dam}}{d_c}} \text{ ungated spillway} \qquad (1)$$

$$\frac{\Delta H}{H_{max}} = 1 - \frac{\frac{d_1}{d_c} + \frac{1}{2}\left(\frac{d_c}{d_1}\right)^2}{\frac{H_{max} + H_o}{d_c}} \text{ gated spillway} \qquad (2)$$

$$\Delta H = H_{max} - H_{res} \qquad (3)$$

Here, ΔH denotes the computed total head loss; $\Delta H/H_{max}$ is the energy dissipation ratio; H_{max} is the peak head given by $H_{max} = H_{dam} + 1.5dc$; H_{dam} is the dam height; and dc is the critical depth computed as $d_c = (q_w^2/g)^{1/3}$.

The residual energy H_{res} comprises both velocity head and pressure head components. When the nappe is aerated and descends freely, the pressure head contribution becomes negligible, and the residual energy is dominated by velocity and potential energy. Accordingly, the total residual energy at a downstream cross-section for a freely falling nappe can be approximated as:

$$H_{res} = \frac{\upsilon_1^2}{2g} + d_1 \qquad (4)$$

This residual energy is subsequently dissipated at the spillway toe through a hydraulic jump in the stilling basin.

For ungated spillways, the maximum available head relates to dam height as:

$$H_{max} = H_{dam} + 1.5d_c \qquad (5)$$

For gated spillways, the relationship between maximum available head and dam height is:

$$H_{max} = H_{dam} + H_o \qquad (6)$$

where H_{dam} is the dam height and H_o is the reservoir free-surface elevation above the spillway crest.

Energy Loss in Skimming Flow Regime

Energy is expended in sustaining stable recirculating vortices within the step cavities. Chanson (1994, 1994a) states that under steady downstream flow conditions (Figure 5), the energy loss can be expressed as:

$$\frac{\Delta H}{H_{max}} = 1 - \frac{\left(\frac{d_w}{d_c}\right)\cos\theta + \frac{1}{2}\left(\frac{d_c}{d_w}\right)^2}{\frac{H_{dam}}{d_c} + \frac{3}{2}} \qquad (7)$$

In this expression, $\Delta H/H_{max}$ denotes the energy dissipation ratio; ΔH is the total head loss expressed as $\Delta H = H_{max} - H_{res}$; H_{dam} is the dam height; H_{max} is the maximum head estimated as $H_{max} = H_{dam} + 1.5dc$; H_{res} is the residual head given by $H_{res} = \frac{U_{avg}^2}{2g} + d_w \cos\theta$ is the total volumetric discharge; b is the channel width; q_w is the unit discharge computed as $q_w = Q_w/b$; dc is the critical depth approximated as $d_c = (q_w^2)^{1/3}/g$; U_{avg} is the cross-sectional mean velocity calculated as $U_{avg} = q_w/d_w$; d_w is the equivalent clear-water depth calculated as $d_w = \int_{y_0}^{y_{90}}(1 - C)dy$; θ is the channel slope in degrees; and the overall head loss is reformulated

in terms of the friction factor, f, and the spillway slope, θ.

Equation (8) is defined at θ = 52°. The friction factor f = 0.3 represents the mean flow resistance on smooth spillways, while f = 1.30 characterizes the mean flow resistance on stepped spillways.

$$\frac{\Delta H}{H_{max}} = 1 - \frac{\left(\frac{f}{8sin\theta}\right)^{1/3} cos\theta + \frac{E}{2}\left(\frac{f}{8sin\theta}\right)^{-2/3}}{\frac{H_{dam}}{d_c} + \frac{3}{2}} \qquad (8)$$

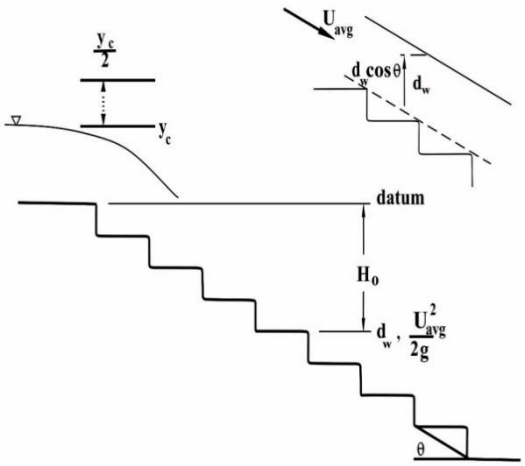

Figure 5. Spillway arrangement with variable definitions

MATERIAL AND METHODS

Eleven studies focusing on horizontal stepped spillways were carefully selected for analysis. These studies shared consistent characteristics: minimum step heights of 3 cm and Froude numbers yielding dimensionless discharge heights corresponding to Reynolds numbers in the range of 1×10^5 to 1×10^6. Large-scale experimental facilities were employed in all selected studies to reduce scale effects on air-water flow behavior under high-velocity free-surface conditions. Air-water flow properties at the outer edge of each step, downstream of the air-entrainment inception point, were characterized using intrusive conductivity phase-detection probes alongside optical fiber probes. Flow velocity assessment was performed using Dall Tube flow meters, V-notch measurements, and Prandtl-Pitot devices, while point gauges were used to determine clear-water flow depth, accounting for the challenges introduced by substantial air entrainment at the air-water interface.

The conductivity probe exploits the resistivity contrast between air and water, producing an instantaneous voltage output. Signal processing via the threshold method applied to a single sensor yield: (a) the time-averaged local void fraction C, (b) the bubble count rate F representing the frequency of phase transitions between air and water, and (c) the chord lengths of air bubbles and water droplets. For a dual-tip conductivity probe with sensors offset longitudinally, cross-correlation of the two signals provides the local time-averaged interfacial velocity V. Further detail on signal processing methodology is available in the cited references. The dual-tip probes employed had sensor tip diameters of Ø = 0.13 mm and 0.25 mm, with data acquisition conducted over 45-

second intervals at a sampling rate of 20 kHz per sensor. Tested flow rates encompassed transition and skimming conditions of $0.035 \leq q_w \leq 0.234$ m²/s for $\theta = 8.9°$ and $0.02 \leq q_w \leq 0.249$ m²/s for $\theta = 26.6°$, with corresponding Reynolds numbers of $1.4\times10^5 \leq Re \leq 9.3\times10^5$ and $8.1\times10^4 \leq Re \leq 9.9\times10^5$, respectively.

Large-scale experimental configurations were adopted to minimize scale-related distortions in the micro-scale dynamics of air-water flow under high-velocity free-surface conditions. Scale effects arise when secondary forces — namely viscous forces and surface tension — are neglected in physical models. Although these forces are typically disregarded in standard open-channel flow scenarios, they become critically important in the highly aerated flows characteristic of stepped spillways, and their omission can yield erroneous interpretations of experimental data. The influence of scale effects in stepped spillway modeling has been thoroughly investigated by Boes (2000), Chanson (2002), Boes and Hager (2003a), and Takahashi et al. (2005). In general, scale effects become most pronounced at model scales smaller than 10:1. Strategies for mitigating scale effects are outlined in Chanson (2002), Boes and Hager (2003a), and Takahashi et al. (2006). Chanson (2002) advocates for a minimum model scale of 10:1, while Boes and Hager (2003a) recommend maintaining a minimum Reynolds number of 10^5 and a minimum Weber number of 100.

Takahashi et al. (2006) emphasize that simultaneous adherence to Froude, Reynolds, and Morton similarity criteria is required when modeling flows with significant air entrainment, and that this condition can only be fully satisfied at full scale. Although no universal consensus has emerged among researchers regarding the criteria for managing scale effects in stepped spillway physical models, several practical guidelines are available. Conventional single-phase flow instrumentation has proven inadequate for characterizing high-velocity air-water mixtures owing to the complex three-dimensional flow structure and intense air-water interactions involved.

Given the pronounced air entrainment at the air-water interface, instruments such as Dall Tube flow meters, V-notch weirs, Prandtl-Pitot tubes, and clear-water point gauges are unsuitable for characterizing air-water flow properties in stepped spillway environments. Intrusive probes are therefore commonly employed, and experimental investigations using optical fiber and conductivity probes have produced reliable and reproducible results.

a) Development of the Models

Approximately 500 comprehensive data cases were analyzed to develop energy dissipation models applicable to transition and skimming flow under varying operational conditions. A critical step in model development is the identification of parameter values that accurately characterize the modeled system.

Applying the least squares fitting procedure, the optimal regression relationship for this study was formulated as:

$$\frac{\Delta H}{H_{max}} = \left[\alpha_0 \frac{Nh}{y_c}\right]^{\alpha_1} N^{\alpha_2} h^{\alpha_3} \theta^{\alpha_4} \quad (9)$$

Where:

- $\Delta H/H_{max}$ is the energy dissipation ratio,
- H_{max} is the maximum available head,
- N is the total number of spillway steps,
- h is the individual step height,
- θ is the spillway channel slope,
- α_0, α_1, α_2, α_3, and α_4 are regression coefficients.

A portion of the compiled dataset was used in conjunction with multiple regression analysis and matrix solution techniques to solve Equation (9), yielding the constant α_0 and coefficients α_1

through α_4. These values were subsequently incorporated to derive the models presented in Section 3.

b) Model Validation

The remaining and independent validation datasets were used to assess model performance through interpolation testing. Accurate representation of the validation data indicates that the model faithfully reflects real system behavior — a quality referred to as interpolation fidelity.

The Pearson Correlation Coefficient was adopted as the primary statistical metric for evaluating model reliability. This coefficient quantifies the nature of the linear relationship between two variables on a scale from −1 to +1: a value of −1 denotes a perfect negative correlation, 0 indicates no linear association, and +1 reflects a perfect positive correlation. The Pearson coefficient was computed manually using the following formula (Stephanie Glen, 2020):

$$r = \frac{n\sum xy - \sum x \sum y}{\sqrt{\left(n\sum x^2 - (\sum x)^2\right)(n\sum y^2 - (\sum y)^2)}} \qquad (10)$$

Where:

- x and y are the values of the two variables,
- n is the number of paired observations,
- $\sum x$ is the sum of all x values,
- $\sum y$ is the sum of all y values,
- $\sum x^2$ is the sum of squared x values,
- $\sum y^2$ is the sum of squared y values,
- $\sum xy$ is the sum of the products of corresponding x and y values.

FINDINGS

Established Models for the Transition/Skimming Flow Regime

Flow rates recorded during testing spanned transition and skimming conditions of 0.035 to 0.234 m²/s for θ = 8.9°, and 0.02 to 0.249 m²/s for θ = 26.6°. Measured Reynolds numbers ranged from 1.4×10^5 to 9.3×10^5 for θ = 8.9°, and from 8.1×10^4 to 9.9×10^5 for θ = 26.6°.

The developed model and its variants (Eqs. 11–19) were subsequently applied to predict energy dissipation rates, and the resulting predictions were plotted against the measured datasets in Figures 6 through 14.

θ = 26.6°, N = 10, h (cm) = 10

$$\Delta H/H_{max} = (0.136\, Nh/d_c)^{0.77} N^{-0.12} h^{-0.36} \theta^{0.22} \qquad \textbf{(11)}$$

At θ = 26.6°, the applicable parameter ranges are: Nh/dc from 5.0 to 10.0, N from 5 to 20, dc/h from 0.80 to 3.30, and h = 10 cm, confirming suitability for flat stepped spillways. A Spearman coefficient of 0.97 reflects strong predictive agreement between the model and observed data, as depicted in Figure 6, affirming the model's utility as a reliable design and research tool.

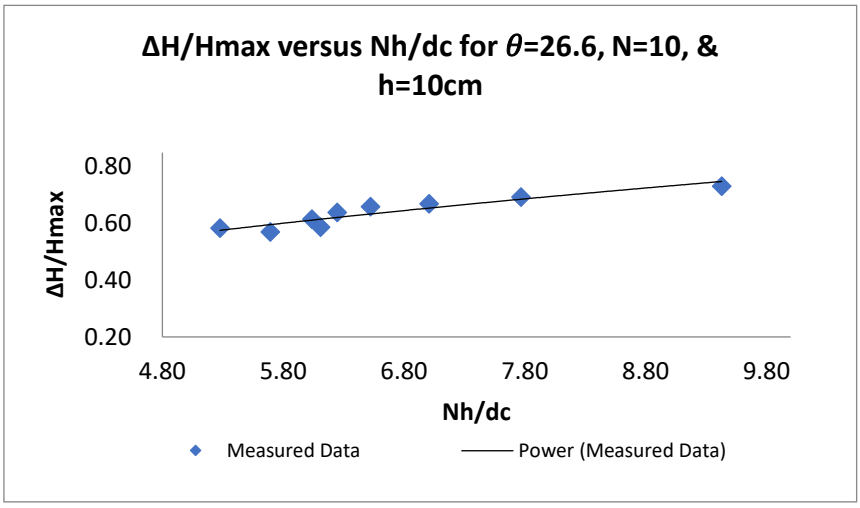

Figure 6: $\Delta H/H_{max}$ as a function of Nh/dc between 5.00 and 10.00, q_w = (0.073–0.249) m²/s, Re = (2.92×10^5–9.96×10^5), dc/h = (0.82–1.85).

θ = 26.6°, N = 20, h (cm) = 5

$$\Delta H/H_{max} = (0.08\, Nh/d_c)^{0.77} N^{-0.12} h^{-0.36} \theta^{0.22} \quad \textbf{(12)}$$

This equation applies for θ from 21.8° to 26.6°, Nh/dc from 5.0 to 25, N from 5 to 20, dc/h from 0.80 to 1.85, and h from 5 to 10 cm. The Spearman coefficient of 0.94 confirms strong agreement between the model and the data, as illustrated in Figure 7.

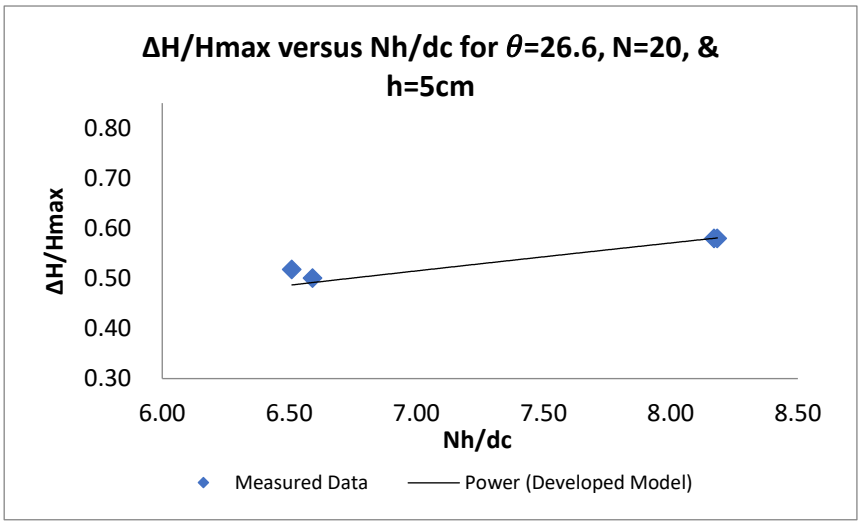

Figure 7: $\Delta H/H_{max}$ plotted against Nh/dc from 4.00 to 10.00, q_w = (0.020–0.227) m²/s, Re = (8.0×10^4–9.08×10^5), dc/h = (0.69–3.30).

θ = 21.8°, N = 10, h (cm) = 10

$$\Delta H/H_{max} = (0.11\, Nh/d_c)^{0.77} N^{-0.12} h^{-0.36} \theta^{0.22} \quad (13)$$

At θ = 21.8°, the parameter ranges are: Nh/dc from 5.0 to 10.0, N from 5 to 20, dc/h from 0.80 to 3.30, and h = 10 cm. A Spearman coefficient of 0.90 demonstrates robust model performance, as shown in Figure 8, validating the model for this slope configuration.

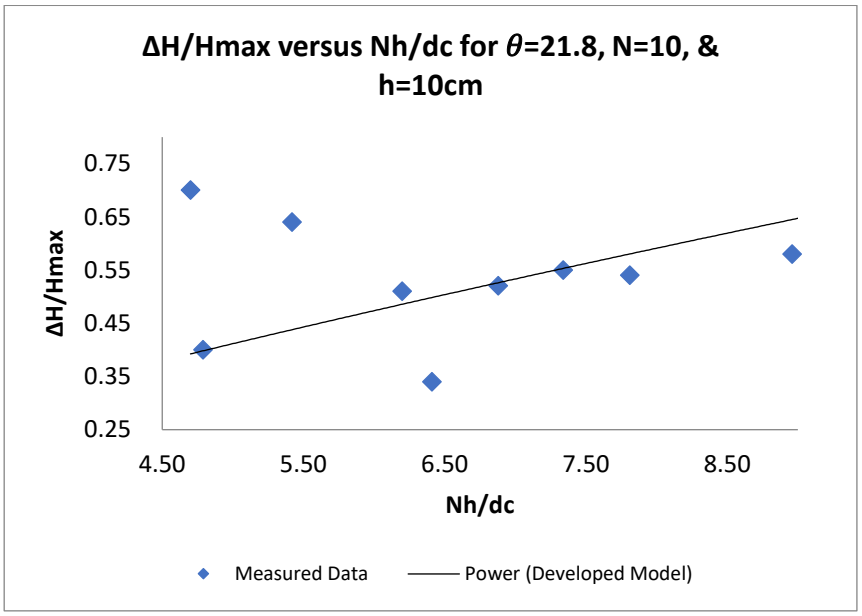

Figure 8: $\Delta H/H_{max}$ plotted against Nh/dc spanning 5.00 to 12.00, q_w = (0.095–0.180) m²/s, Re = (3.80×10⁵–7.20×10⁵), dc/h = (1.00–1.57).

θ = 21.8°, N = 20, h (cm) = 5

$$\Delta H/H_{max} = (0.11\, Nh/d_c)^{0.77} N^{-0.12} h^{-0.36} \theta^{0.22} \quad (14)$$

At θ = 21.8°, Nh/dc ranges from 5.0 to 12.0, N from 10 to 20, dc/h from 0.80 to 3.30, and h = 10 cm. The Spearman coefficient of 0.90 confirms a notable correspondence between observed and modeled values, as presented in Figure 9.

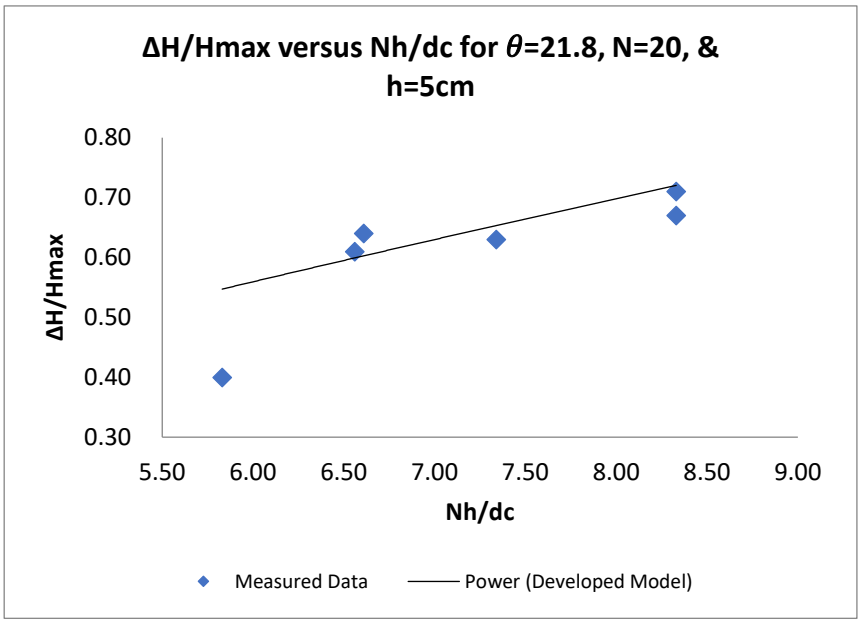

Figure 9: $\Delta H/H_{max}$ as a function of Nh/dc ranging from 5.00 to 12.00, q_w = (0.095–0.180) m²/s, Re = (3.80×10⁵–7.20×10⁵), dc/h = (1.00–1.57).

θ = 18.4°, N = 40, h (cm) = 6

$$\Delta H/H_{max} = (0055\, Nh/d_c)^{0.77} N^{-0.12} h^{-0.36} \theta^{0.22} \quad (15)$$

At θ = 18.4°, Nh/dc values fall between 5.0 and 10.0, N ranges from 20 to 40, dc/h from 0.80 to 3.30, and h = 6 cm. The Spearman coefficient of 0.95 confirms strong model-data alignment, as depicted in Figure 10, supporting the model's applicability for this configuration.

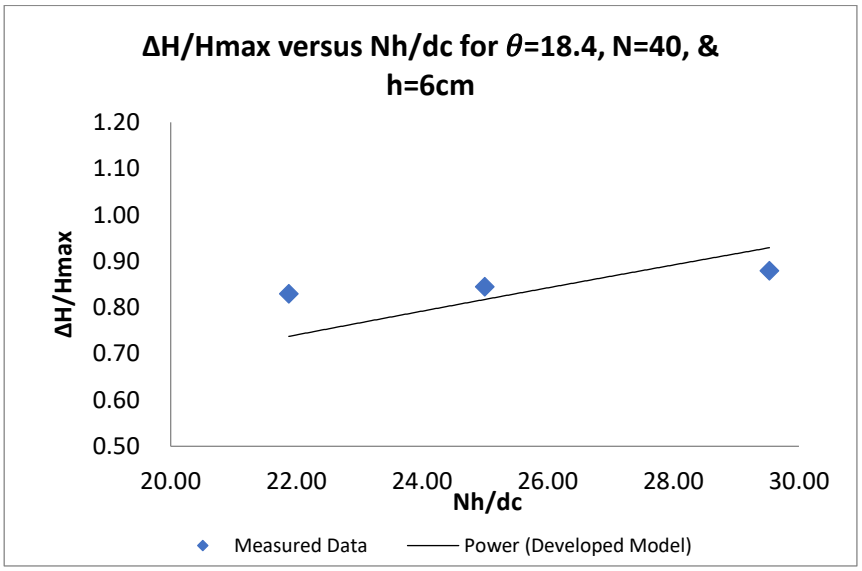

Figure 10: $\Delta H/H_{max}$ as a function of Nh/dc between 5.50 and 11.00, q_w = (0.059–0.158) m²/s, Re = (2.36×10⁵–6.32×10⁵), dc/h = (0.80–1.85).

θ = 15.9°, N = 18, h (cm) = 5

$$\Delta H/H_{max} = (0.09\, Nh/d_c)^{0.77} N^{-0.12} h^{-0.36} \theta^{0.22} \quad (16)$$

At θ = 15.9°, the applicable ranges are: Nh/dc from 5.0 to 10.0, N from 5 to 20, dc/h from 0.80 to 3.30, and h = 5 cm. A Spearman coefficient of 0.79, while the lowest among the models, still reflects an acceptable level of predictive agreement, as illustrated in Figure 11.

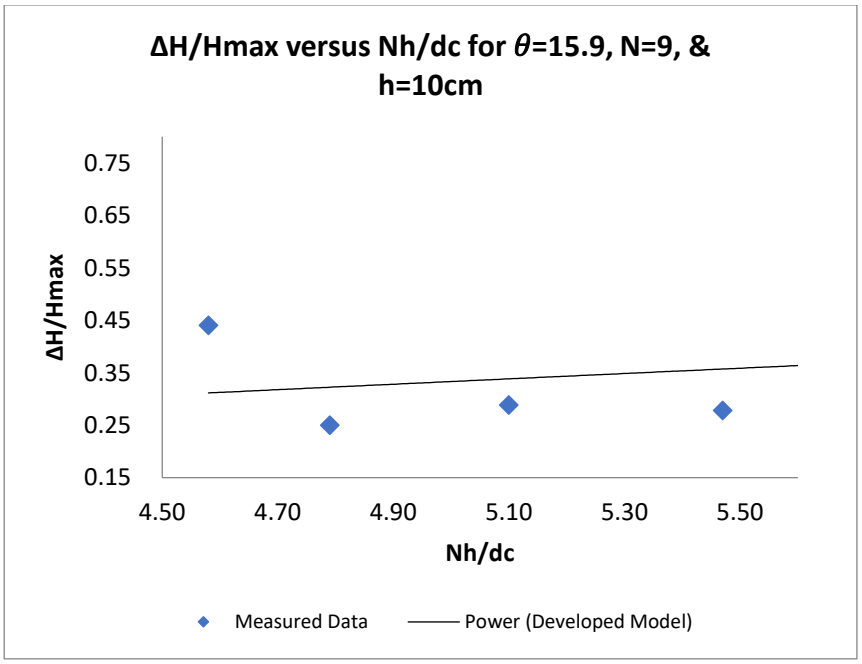

Figure 11: $\Delta H/H_{max}$ as a function of Nh/dc between 4.50 and 6.60, q_w = (0.069–0.188) m²/s, Re = (2.76×10⁵–7.52×10⁵), dc/h = (0.78–1.53).

θ = 14.6°, N = 13, h (cm) = 10

$$\Delta H/H_{max} = (0.09\,Nh/d_c)^{0.77} N^{-0.12} h^{-0.36} \theta^{0.22} \quad (17)$$

At θ = 14.6°, Nh/dc ranges from 5.0 to 10.0, N from 5 to 20, dc/h from 0.80 to 3.30, and h = 10 cm. A Spearman coefficient of 1.0 reflects perfect correlation between observed and predicted values, as shown in Figure 12, confirming excellent model fidelity for this slope.

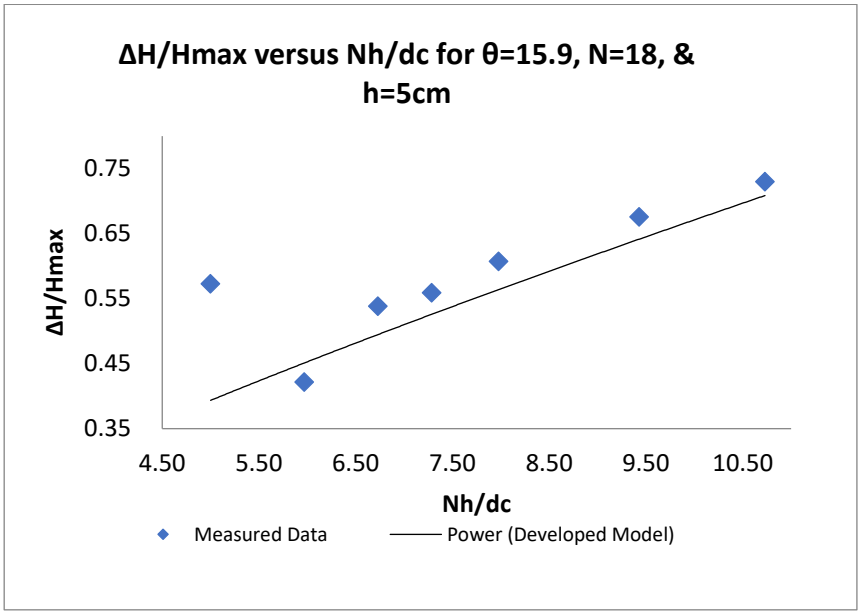

Figure 12: $\Delta H/H_{max}$ as a function of Nh/dc between 6.25 and 8.60, q_w = (0.069–0.188) m²/s, Re = (2.76×10⁵–7.52×10⁵).

θ = 14.6°, N = 26, h (cm) = 5

$$\Delta H/H_{max} = (0.15\,Nh/d_c)^{0.77} N^{-0.12} h^{-0.36} \theta^{0.22} \quad (18)$$

At θ = 14.6°, Nh/dc values range from 5.0 to 10.0, N from 5 to 20, dc/h from 0.80 to 3.30, and h = 26 cm. The Spearman coefficient of 0.93 reflects a strong and meaningful association between actual data and model predictions, as illustrated in Figure 13.

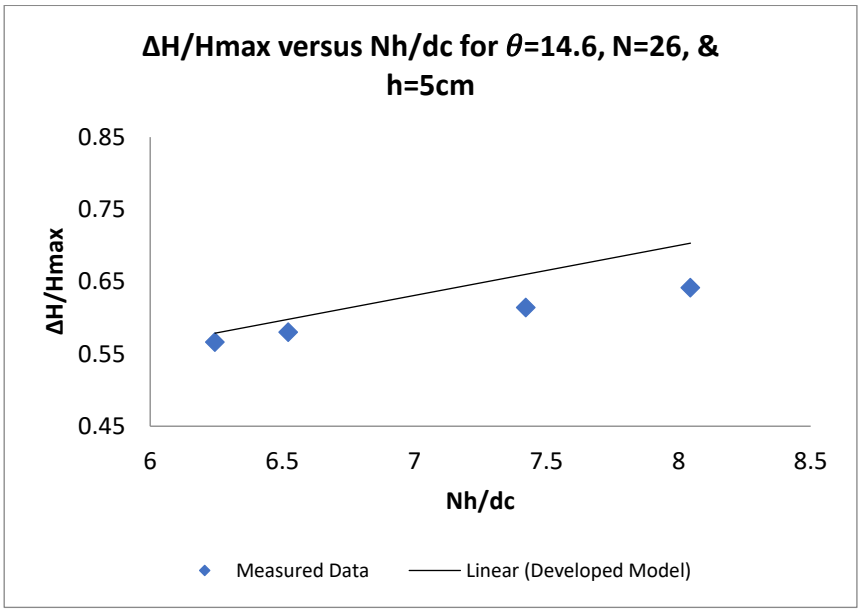

Figure 13: $\Delta H/H_{max}$ related to Nh/dc values between 6.20 and 8.00, q_w = (0.05–0.234) m²/s, Re = (2.0×10⁵–9.36×10⁵), dc/h = (1.27–3.55).

θ = 8.9°, N = 21, h (cm) = 3/6

$$\Delta H/H_{max} = (0.17\, Nh/d_c)^{0.77} N^{-0.12} h^{-0.36} \theta^{0.22} \quad (19)$$

At θ = 8.9°, Nh/dc ranges from 4.5 to 25.0, N from 5 to 20, dc/h from 0.80 to 3.30, and h = 21 cm. A Spearman coefficient of 1.0 confirms perfect predictive accuracy for this configuration, as demonstrated in Figure 14, underscoring the model's robustness at the lower end of the slope range.

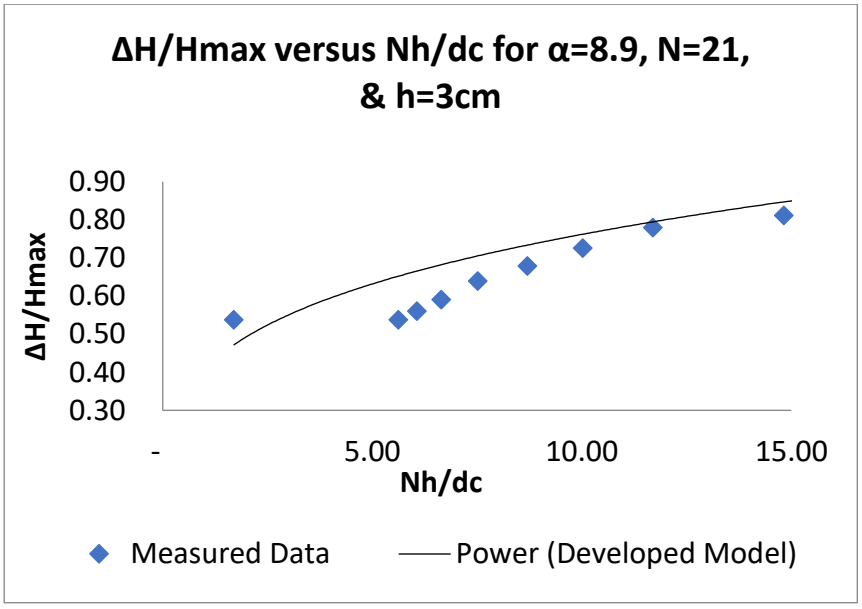

Figure 14: $\Delta H/H_{max}$ as a function of Nh/dc values between 5.00 and 12.00, qw = (0.035–0.234) m²/s, Re = (1.40×10⁵–9.36×10⁵).

4. RESULT AND DISCUSSION

The compiled data and the analytical models derived from Equations (11) to (19) characterize energy dissipation ratios as a function of dam height relative to critical depth, as illustrated in Figures 6 through 14. The proposed models

demonstrated strong agreement with the energy dissipation measurements, yielding Spearman coefficients spanning 0.79 to 1.0. As evident from Figures 6 through 14, energy losses at a given discharge increase with dam height, a trend consistent with findings reported in the literature. The dimensionless energy dissipation rates exhibit strong correspondence with both transition and skimming flow regimes across all evaluated datasets. Pearson correlation coefficients ranging from 0.79 to 1.00 confirm that both flow regimes, as captured in Figures 9 through 15, are well-represented by Equations (11) to (19).

5. CONCLUSION

Energy losses derived from both measured and predicted datasets, expressed as a function of the dam height-to-critical depth ratio, are presented in each figure. In agreement with prior findings, the distribution of both datasets follows a characteristic concave profile. Energy losses at specified discharges increase proportionally with dam height, consistent with recent literature. Spearman correlation coefficients ranging from 0.79 to 1.00 demonstrate a strong and consistent relationship between estimated and observed values, affirming the model's capacity to reliably predict flow characteristics across the defined parameter space. The proposed model and its variants are designed to be intuitive, computationally straightforward, and capable of delivering accurate results for practical engineering applications.

6. DESIGN APPLICATION

Question: Given a unit discharge of 0.015 m²/s, with 21 steps, a step height of 0.05 m, and a step length of 0.319 m, determine the energy dissipated at the toe of a stepped spillway.

Solution: Convert the step height to centimeters as required by the model: h = 0.05 m = 5 cm.

Given:

- N = 21
- Tan θ = 0.05m/0.315m
- θ = 8.9°
- h = 0.05 m (5 cm for model input)
- q_w =0. 015 m²/s
- d_c = (0.015²/9.81) ^0.33 = 0.03 m,
- dc/h = 0.03/5 = 0.006
- Nh/dc = 21 × 5/0.03 = 3500

Substituting into Equation (19):

$\Delta H/H_{max} = (0.17 * 3500)^{0.77} * 21^{-0.12} * 5^{-0.36} * 8.9^{0.22} = 86\%$

LIST OF SYMBOLS

The following symbols are used in this paper:

- **C** — void fraction, defined as the volume of air per unit volume of the air-water mixture; also referred to as air concentration or local air content
- **D_H** — hydraulic diameter (m)
- **d_w** — equivalent clear-water flow depth (m)
- **dc** — critical flow depth (m)
- **g** — gravitational acceleration (m/s²)
- **H** — total head (m)
- **H_{dam}** — dam height (m)
- **H_{max}** — maximum upstream head (m) above the chute toe: $H_{max} = H_{dam} + 1.5dc$
- **H_{res}** — residual head (m)
- **h** — vertical step height (m)
- **l** — horizontal step length (m)
- **q_w** — water discharge per unit width (m²/s)

Re — Reynolds number defined in terms of hydraulic diameter: $Re = \rho_w \times U_w \times D_H/\mu_w$;**$U_w$**

U_w - mean flow velocity (m/s): $U_w = q_w/d$;

- **U_{avg}** — cross-sectional average flow velocity (m/s) for stepped spillway
- **W** — channel width (m)
- **Y_{90}** — characteristic depth (m) at which the void fraction equals 90%
- **D** — distance (m) measured normal to the invert (or channel bed)
- **ΔH** — total head loss (m): $\Delta H = H_{max} - Hres$
- **θ** — angle between the pseudo-bottom formed by the step edges and the horizontal

Subscripts

- **c** — critical flow conditions
- **max** — maximum value
- **mean** — mean signal component
- **w** — water properties

REFERENCES

[1] Chanson, H. "The hydraulics of stepped chutes and spillways," Balkema, 2001.

[2] Chamani, R, and Rajaratnam, N. "Jet flow on stepped spillways," J. Hydraul. Eng., vol. 120, no. 2, pp. 254-259, 1994.

[3] Kramer, M. and Chanson, H. "Transition flow regime on stepped spillways: Air-water flow characteristics and step-cavity fluctuations," Environ. Fluid Mech., vol. 18, no. 4, pp. 947-965, 2018.

[4] Ozueigbo, O. "Using a ball that bounces down a flight of stairs to determine energy dissipation in stepped spillway with a fully developed hydraulic jump," J. Eng. Res. Rep., 2022, doi: 10.9734/jerr/2022/v23i417604.

[5] Chanson, H. and Toombes, L. "Air-water flows down stepped chutes: Turbulence and flow structure observations," Int. J. Multiphase Flow, vol. 28, no. 11, pp. 1737-1761, 2002.

[6] Chanson, H. and Toombes, L. "Energy dissipation and air entrainment in stepped storm waterway: Experimental study," J. Irrig. Drain. Eng., vol. 128, no. 5, pp. 305-315, 2002.

[7] Stephenson, D. "Energy dissipation down stepped spillways," Int. Water Power Dam Constr., pp. 27-30, 1991.

[8] Ozueigbo, O. and Agunwamba, J. "Two new equations for energy dissipation down a stepped spillway with channel slopes between 3.4° and 26.6°," in Techniques and Innovation in Engineering Research, 2023, doi: 10.9734/bpi/taier/v8/3589C.

[9] Chanson, H. "Measuring air-water interface area in supercritical open channel flow," Water Res., vol. 31, no. 6, pp. 1414-1420, 1997.

[10] Chanson, H. "Comparison of energy dissipation between nappe and skimming flow regimes on stepped chutes," J. Hydraul. Res., vol. 32, no. 2, pp. 213-218, 1994.

[11] Sorensen, M. "Stepped spillway hydraulic model investigation," J. Hydraul. Eng., vol. 111, no. 12, pp. 1461-14725, 1985.

[12] Ozueigbo, O. and Agunwamba, J. "New equations for energy dissipation down a stepped spillway," J. Eng. Res. Rep., 2022, doi: 10.9734/JERR/2022/v23i417602.

[13] Essery, I. T. and Horner, M. W. "The hydraulic design of stepped spillways," Construction Industry Research and Information Association, London, U.K., Rep. 33, 2005.

[14] Takahashi, M. Yasuda, Y. and Ohtsu, I. "Flow patterns and energy dissipation over various stepped chutes," J. Irrig. Drain. Eng., vol. 134, no. 1, pp. 114-116, 2008.

[15] Chanson, H. "Air bubble entrainment in open channels. Flow structure and bubble size distributions," Int. J. Multiphase Flow, vol. 23, no. 1, pp. 193-203, 1997.

[16] Felder, S. and Chanson, H. "Energy dissipation, flow resistance and gas-liquid interfacial area in skimming flows on moderate-slope stepped spillways," Environ. Fluid Mech., vol. 9, no. 4, pp. 427-441, 2009.

[17] Bahmanpouri, F. and Gualtieri, C. "Experiments on two-phase flow in hydraulic jump on pebbled rough bed: Part 1–Turbulence properties and particle chord time and length," Water Sci. Eng., 2023, doi: 10.1016/j.wse.2023.01.001.

[18] Ozueigbo, O. "Three new approaches to estimating energy losses in stepped spillways with the channel slope of 8.9°," J. Eng. Res. Rep., 2025, doi: 10.9734/jerr/2025/v27i31426.

[19] Gualtieri et al., "Application of the entropy model to estimate flow discharge and bed load transport in a large river," Phys. Fluids, 2025

[20] Agunwamba, J. “Engineering mathematical analysis,” Enugu: De – Adroit Innovation, Chapter Twelve, 2007, pp. 479–510, 674–675.

[21] Stephanie, G. “Alpha level (significance level): What is it?,” StatisticsHowTo.com: Elementary Statistics for the rest of us!, https://www.statisticshowto.com/probability-and-statistics/statistics-definitions/what-is-an-alpha-level/, 2018.